Geol. Mag. **138** (*3*), *2001, pp. 237–251. Printed in the United Kingdom* © *2001 Cambridge University Press*

The early Palaeozoic magmatic event in the Northwest Himalaya, India: source, tectonic setting and age of emplacement

C. MILLER*, M. THÖNI†, W. FRANK†, B. GRASEMANN†, U. KLÖTZLI†, P. GUNTLI‡ & E. DRAGANITS†

*Institut für Mineralogie und Petrographie, University of Innsbruck, Innrain 52, A-6020 Innsbruck, Austria
†Institut für Geologie, University of Vienna, Althanstrasse 14, A-1090 Vienna, Austria
‡Sieber Cassina & Handke AG, CH-7000 Chur, Switzerland

(*Received* 30 May 2000; *accepted* 31 January 2001)

Abstract – In the High Himalayan Crystalline Series of Northwest India, numerous peraluminous granites intruded the metasediments of the late Proterozoic to early late Cambrian Haimanta Group. Nd and Sr isotope systematics confirm that they were derived from heterogeneous crustal sources. New geochronological data from two plutons range in age from late Precambrian to early Ordovician: single zircon U–Pb dating yielded an age of 553 ± 2 (2σ) Ma for the Kaplas granite, whereas mineral Sm–Nd isotope systematics define a crystallization age of 496 ± 14 (2σ) Ma for the tholeiitic mafic rocks in the Mandi pluton, where evidence of magma mingling documents a close association between mafic and granitic melts. The end of this period of magmatic activity coincides with the depositional gap below the Ordovician transgression, caused by surface uplift and erosion, that is an important feature in the stratigraphy of the Northwest Himalaya. In Spiti, the transgression of the Ordovician basal conglomerates on a normal fault indicates pre-Ordovician extensional faulting. Therefore, the early Palaeozoic magmatic activities in the Northwest Himalaya could be correlated with a late extensional stage of the long-lasting Pan-African orogenic cycle which ended with the formation of the Gondwana supercontinent.

1. Introduction

The Himalayan–Tibetan orogen was created by the collision of the Eurasian and Indian plates over the past 50–70 Ma. Subduction of the Indian plate has resulted in a series of late Cenozoic northward-dipping fault systems which can be observed for 2000 km along strike of the orogen. They separate the Himalaya into three tectonic units: (1) The structurally lowest Lesser Himalaya is bounded by the Main Boundary Thrust below and by the Main Central Thrust (Heim & Gansser, 1939; Gansser, 1964) above. Low-grade metasediments, mainly Precambrian–early Palaeozoic in age, predominate. (2) The High Himalayan Crystalline Series is bounded by the Main Central Thrust at the base and by the South Tibetan Detachment fault (Burg & Chen, 1984) at the top. It is a belt of mostly high-grade late Proterozoic to early Palaeozoic metasedimentary and granitic rocks, intruded by Miocene leucogranites. (3) The North Himalaya or Tibetan Zone comprises latest Proterozoic to Eocene continental margin sequences (Gaetani & Garzanti, 1991) and lies between the South Tibetan Detachment fault and the Indus-Yarlung Suture which marks the zone of collision. These three units are considered to be parts of the former northern passive margin of India (Brookfield, 1993). Both the High Himalaya and the North Himalaya were intruded by numerous late Proterozoic to Ordovician granites (Table 1). The processes responsible for these intrusions are important for models of the evolution of the pre-collision margin, but still controversial. They may have been associated with the assemblage of Gondwana (Gaetani & Garzanti, 1991) or with supercontinent breakup (Murphy & Nance, 1991; Hughes & Jell, 1999). In contrast, the meta-igneous rocks in the Lesser Himalayan Series are exclusively early Proterozoic (Miller *et al.* 2000).

This paper presents single zircon U–Pb data that give a latest Proterozoic age for the Kaplas pluton (Fig. 1). New results from geochemical and isotopic (Sr and Nd) studies of granitoids and associated mafic rocks, in particular for the Mandi plutonic unit (Fig. 1), constrain source characteristics of the early Palaeozoic magmatic event in the Northwest Himalaya and the complex early history of this part of the Himalayan orogen.

2. Analytical methods

Nd and Sm concentrations were determined by isotope dilution, using a mixed ^{147}Sm–^{150}Nd spike, and run as metals on a Finnigan MAT 262 multicollector

* Author for correspondence: Christine.Miller@uibk.ac.at

Table 1. Published age data of late Precambrian to early Palaeozoic magmatic rocks from the High Himalaya Crystalline Series and the North Himalaya

Segment	Location		Rock type	Method		Age (Ma)	$^{87}Sr/^{86}Sr(i)$	Reference
Pakistan	Mansehra		Granite	Rb–Sr	WR	516 ± 16	0.7198 ± 0.0006	Le Fort, Debon & Sonet, 1980
NW India	Mandi	Himachal Pradesh	Granite	Rb–Sr	WR	507 ± 100	0.718 ± 0.025	Jäger, Bhandari & Bhanot, 1971
	Mandi	Himachal Pradesh	Mafic pillow	Sm–Nd	WR–Cpx–Plg	496 ± 14		This study
	Kaplas	Chamba	Granite	U–Pb	Zircon	552 ± 2		This study
	Manikaran	Himachal Pradesh	Granite	Rb–Sr	WR	467 ± 45	0.719	Bhanot *et al.* 1979
	Kullu	Himachal Pradesh	Granite	Rb–Sr	WR	495 ± 16	0.720 ± 0.002	Frank, Thöni & Purtscheller, 1977
	KinnaurKailash	Sutlej,BaspaValley	Granite	U–Pb	Zircon	488 ± 4		Marquer, Chawla & Challandes, 2000
	Kinnaur Kailash	Sutlej, Baspa Valley	Granite	Rb–Sr	WR	453 ± 9	0.7370 ± 0.0020	Kwatra *et al.* 1999
	Hante	Kashmir	Granite	Rb–Sr	WR	489 ± 20	0.717 ± 0.001	Rao *et al.* 1990
	Miyar	Lahul	Orthogneiss	U–Pb	Monazite	479 ± 4		Pognante *et al.* 1990
	Miyar	Lahul	Orthogneiss	Rb–Sr	WR	549 ± 70	0.7175 ± 0.0073	Pognante *et al.* 1990
	Nyimaling	Ladakh	Granite	Rb–Sr	WR	460 ± 8	0.7365 ± 0.0002	Stutz & Thoni, 1987
	Rupshu	Ladakh	Granite	U–Pb	Zircon	483 ± 1		Girard & Bussy, 1999
	TsoMorari	Ladakh	Granite	U–Pb	Zircon	479 ± 2		Girard & Bussy, 1999
	Tso Morari	Ladakh	Gneiss	U–Pb	Zircon	479 ± 2		Girard & Bussy, 1999
	Khadrala	Jutogh	Granite	Rb–Sr	WR	460 ± 18	0.7244 ± 0.0041	Rai *et al.* 1993
	Champawat	Almora nappe	Granodiorite	Rb–Sr	WR	560 ± 20	0.7109 ± 0.0013	Trivedi, Gopalan & Valdiya, 1984
Nepal	Dadeldhura	W Nepal	Granite	Rb–Sr	WR	470 ± 6	0.7266 ± 0.0012	Einfalt, Hoehndorf & Kaphle, 1993
	Simchar	Kathmandu nappe	Granite	Rb–Sr	WR	466 ± 40	0.7205 ± 0.0046	Le Fort, Debon & Sonet, 1983
	Palung	Kathmandu nappe	Granite	U–Pb	Zirc, mnz	470 ± 4		Schärer & Allègre, 1983
	Formation III	Tibetan Slab	Augengneiss	Rb–Sr	WR	513 ± 30	0.711 ± 0.003	Le Fort *et al.* 1986
S Tibet	Kangmar	Lhagoi-Kangri	Granite	U–Pb	Zircon	562 ± 4		Schärer, Xu & Allègre, 1986
	Kangmar	Lhagoi-Kangri	Granite	Rb–Sr	WR	485 ± 6	0.7186 ± 0.0018	Wang *et al.* 1981
	Kangmar	Lhagoi-Kangri	Granite	Rb–Sr	WR	484 ± 7	0.7140 ± 0.0012	Debon *et al.* 1981

WR = whole rock; Zirc = zircon; mnz = monazite; Cpx = clinopyroxene; Plg = plagioclase.

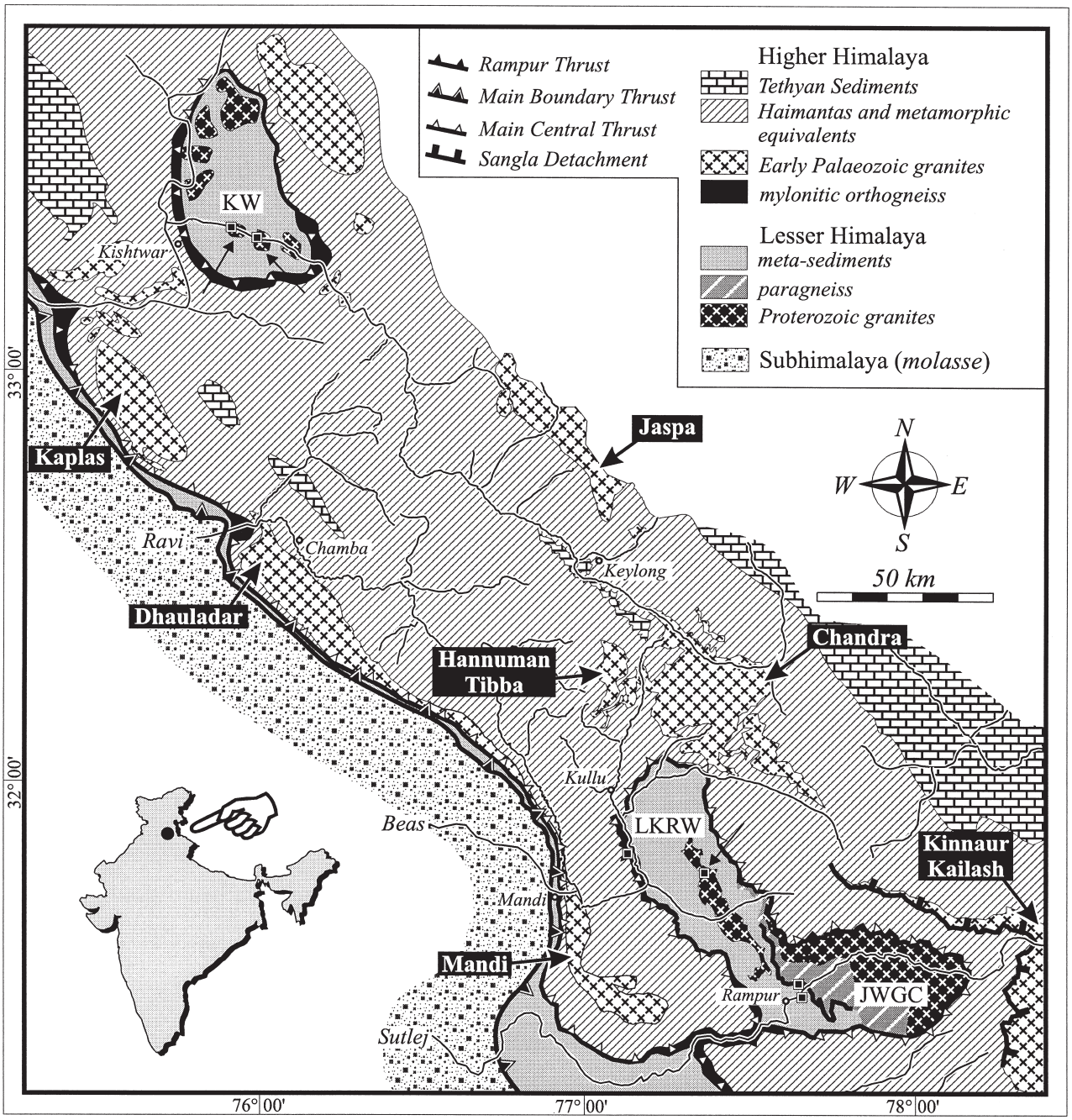

Figure 1. Tectonic cartoon map of the Northwest Himalaya (India), simplified after Frank *et al.* (1995) and Vannay & Grasemann (1998), and sample locations (squares). Small arrows indicate outcrops. Samples from the Nyimaling granite west of Tso Morari are located further to the north and not indicated on this map. JWGC = Jeori-Wangtu Gneiss Complex, KW = Kishtwar Window, LKRW = Larji-Kullu-Rampur Window.

mass spectrometer at the University of Vienna. Nd was ionized using a Re double filament. Within-run isotope fractionation was corrected for $^{146}Nd/^{144}Nd = 0.7219$. All errors quoted in Table 4 correspond to 2 sigma standard errors of the mean. The $^{143}Nd/^{144}Nd$ ratio for the La Jolla international standard during the course of this investigation was 0.511846 ± 8 (35 runs). Errors for the $^{147}Sm/^{144}Nd$ ratio are $\pm$ 1%, or smaller, based on iterative sample analysis and spike recalibration. The following model parameters were used for the calculation of depleted mantle (DM) ages: $^{147}Sm/^{144}Nd = 0.222$, $^{143}Nd/^{144}Nd = 0.513114$ (Michard *et al.* 1985). A linear evolution of the Nd isotope composition of the DM is assumed throughout geological time; εNd values are calculated relative to CHUR.

Zircon pre-chemistry handling (air-abrasion, cleaning) followed procedures given in Krogh (1982). U/Pb analysis followed a modified vapour digestion procedure originally described by Wendt & Todt (1991). U/Pb ratios were determined using a mixed

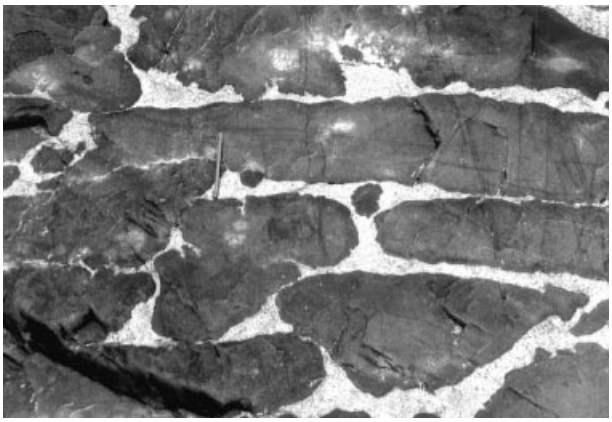

Figure 2. Mafic pillows formed when mafic magma was injected into still-molten granitic magma and was prevented from mixing by rapid quenching of the basalt. Base of photograph is 3 m. Mandi plutonic complex, High Himalayan Crystalline Series, Northwest Himalaya.

^{205}Pb–^{233}U–^{235}U spike. Pb fractionation derived from NIST SRM 981 and 982 standard measurements was 0.107% per mass unit (± 29%). U fractionation was corrected using U500 standard measurements (0.087% per mass unit; ± 17%). U/Pb analysis was controlled by replicate analyses of standard zircon 91500 (Wiedenbeck *et al*. 1995). External reproducibility for U/Pb analysis based on the 91500 standard measurements is 0.2% for $^{207}Pb/^{206}Pb$ (0.07494 ± 0.00015) and 0.25% for $^{206}Pb/^{238}U$ (0.17972 ± 0.00045). The total procedural Pb blank was 2 pg. The corresponding U blank was below 0.1 pg. Age calculation and error statistics follow Parrish *et al*. (1987) and Ludwig (1999). Other analytical procedures are given in Miller *et al*. (1999).

3. Field relations and petrology

In the Northwest Himalaya, biotite or two-mica granites predominate. Their structural and textural features are highly dependent on the metamorphic overprint and structural reworking during the Tertiary orogenic event. Mica-rich schistose enclaves, country-rock xenoliths (esp. quartzite) may be locally abundant. Associated mafic rocks and mafic enclaves are less common.

The Mandi pluton intruded Proterozoic metasediments (Haimanta Group) and now occupies an area of about 30 km^2 (Fig. 1). Most of it is poorly exposed. The dominant lithology is a homogeneous medium- to coarse-grained granite. Where this equigranular granite becomes porphyritic, K-feldspar megacrysts (up to 30 mm in length) are set in a groundmass of quartz, albite, biotite ± muscovite with accessory apatite, zircon, allanite, sphene, ilmenite and a small amount of alteration minerals. An outcrop in the Beas river valley 4 km east of Mandi reveals that mafic magma intruded into the crystallizing granitic magma. Pillows of the mafic phase in the felsic phase with cuspate-lobate shaped contacts, local chilling of the mafic rocks and an abundance of rounded to angular mafic inclusions are indicative of mingling (Fig. 2) at the site of emplacement (Blake *et al.* 1965). The absence of mafic veins cutting the felsic rock, the intricate thin network of felsic veins and the consequent orientation of the cuspate margins pointing into the mafic rocks suggest that the mafic magma, which was chilled against the felsic magma, had a relatively higher viscosity than the granitic magma. Medium-grained interiors of large mafic pillows are ophitic and consist of early-crystallizing olivine ($Fo_{71–73}$), plagioclase (An_{76}), clinopyroxene ($Wo_{47}En_{46}Fs_7$), late-crystallizing amphiboles (Ti-hastingsitic hornblende followed by magnesiohornblende) and rare phlogopite ($Mg = 0.75$). Accessories are ilmenite and apatite. In contrast, fine-grained subophitic mafic rocks contain clinopyroxene rimmed by magnesiohornblende, biotite and plagioclase (An_{62} to An_{44}).

The Kaplas intrusion is a 40 × 12 km body of coarse-grained, K-feldspar-porphyritic biotite ± muscovite granite emplaced into pelitic–psammitic gneisses of the High Himalayan Crystalline Series in southeast Kashmir (Fig. 1). It contains enclaves of biotite gneiss and is cut by aplite and tourmaline–pegmatite veins. Along the southwest margin a contact aureole has been preserved at the base of the granite. The inner part of this aureole is characterized by migmatites, whereas andalusite–sillimanite–garnet-hornfelses have developed in the outer part.

In Chamba, Kullu, southern Lahul and south of the confluence of the upper Chandra and the Bara Shigri, the upper Proterozoic metasediments of the Haimanta Group were intruded by numerous granitic plutons (e.g. Dhauladar, Baragran, Hanuman Tibba, Manikaran, Jaspa). Rock types include foliated and non-foliated biotite and two-mica granites, tourmaline-bearing leucogranites, granophyres, garnet–muscovite pegmatites and aplites. These granites may contain microgranular and gabbroic mafic enclaves and country rock xenoliths. The presence of andalusite in contact aureoles reflects shallow crustal levels of emplacement.

The Kinnaur Kailas granite (Fig. 1) intrudes metasedimentary rocks of the Haimanta Group (Sharma, 1983). Numerous centimetre/decimetre-sized xenoliths of metasediments within the granite, as well as granitic dykes intruding the metasediments, are observed along the contacts, although the basal contact has been overprinted by mylonitic shear zones (Vannay & Grasemann, 1998). The dominant rock type is a medium- to coarse-grained, often porphyritic biotite monzogranite, containing white alkali-feldspar megacrysts. Fine- to medium-grained tourmaline–muscovite leucogranites occur as discrete intrusions. Muscovite, tourmaline and garnet ($Spess_{26–28}$) are common minerals in pegmatitic dykes. Accessory

Table 2. Major (wt %), trace element and REE (ppm) concentrations of Mandi granitic and mafic rocks, Northwest Himalaya

Sample no.	KAW883	HF67/91	HF63/91	HF64/91	HF94/90	HF59/91	HF61/91	HF66b/91	HF95/90
Lithology	Granite	Granite	Granite	Granodiorite	Qtz-diorite	Mafic pillow	Mafic pillow	Mafic pillow	Mafic pillow
Location	Mandi	Mandi	Mandi	Mandi	Mandi	Mandi	Mandi	Mandi	Mandi
SiO_2	74.28	75.45	71.45	66.38	59.25	48.77	51.11	50.81	48.69
TiO_2	0.13	0.13	0.55	0.86	1.03	1.45	0.69	1.53	1.09
Al_2O_3	13.81	13.85	12.52	15.70	15.94	16.34	15.94	17.37	16.93
Fe_2O_3	1.27	1.38	3.21	4.09	6.09	9.56	6.39	8.57	8.46
MnO	0.02	0.01	0.02	0.03	0.10	0.15	0.07	0.10	0.13
MgO	0.14	0.08	0.97	1.29	3.67	8.30	9.65	6.93	9.29
CaO	0.58	0.58	1.74	2.31	6.20	10.63	11.51	9.41	10.11
Na_2O	3.06	3.14	2.35	2.83	3.20	2.93	2.45	2.96	2.37
K_2O	4.72	4.71	4.71	5.56	2.20	1.10	0.34	1.46	0.43
P_2O_5	0.23	0.22	0.30	0.30	0.22	0.14	0.10	0.15	0.14
LOI	0.69	0.84	0.67	0.61	0.82	0.70	0.31	0.80	0.77
Total	98.93	100.39	98.49	99.96	98.72	100.07	98.56	100.09	98.41
F	2360	n.d.	n.d.	n.d.	863	n.d.	n.d.	n.d.	233
Be	3.3	3.4	3.4	4.9	3.1	1.4	0.7	2.0	0.6
Sc	2	n.d.	n.d.	n.d.	23	n.d.	n.d.	10	5
V	4	7	46.	56	143	210	134	168	165
Cr	36	29	51.	43	127	326	525	273	242
Co	6	1	7	74	39	41	34	43	
Ni	2	6	7	9	25	95	159	82	198
Cu	2	6	10	17	11	63	67	57	43
Zn	61	65	70	70	64	102	45	70	57
Ga	2	n.d.	22	23	20	19	n.d.	18	16
Rb	487	467	257	315	155	55	19	76	25
Sr	14	21	114	151	196	249	275	244	270
Y	6	10	17	26	27	29	15	25	21
Zr	39	58	222	408	149	128	71	117	83
Nb	16	19	20	19	3	3	2	5	2
Ba	55	56	445	927	259	119	80	187	53
Hf	0.3	2.5	7.0	13	0.5	4.2	2.1	3.8	1.5
Ta	2.0	3.5	1.5	1.4	5.9	0.28	0.1	0.6	n.d.
Pb	5	29	42	44	n.d.	9	3.9	12	n.d.
Th	11	13	38	79	16	4.5	2.2	7.5	3
U	2.4	3	4	5	4	1.5	0.4	1.9	0.2
La	9	15	58	97	23	10	6	15	7
Ce	21	34	132	218	56	27	16	37	18
Pr	2.7	4.1	15	26	7.2	3.7	2.2	4.8	2.7
Nd	11	15	56	101	29	18	10	22	13
Sm	2.9	3.7	11	16	7.1	4.7	2.6	5.2	3.7
Eu	0.3	0.2	1.1	1.5	1.7	1.5	0.9	1.5	1.2
Gd	3.0	2.6	7.6	11	7.6	4.4	2.4	4.5	4.0
Tb	0.27	0.41	0.91	1.2	0.84	0.77	0.41	0.72	0.6
Dy	1.5	2.0	3.9	5.9	5.1	5.0	2.5	4.3	3.8
Ho	0.2	0.31	0.66	1.00	0.98	1.1	0.57	1.0	0.78
Er	0.6	0.7	1.6	2.5	2.6	2.7	1.5	2.3	2.2
Tm	0.09	0.13	0.19	0.31	0.38	0.39	0.21	0.38	0.31
Yb	0.42	0.7	1.4	2.1	2.38	2.7	1.3	2.4	1.9
Lu	0.07	0.10	0.20	0.29	0.33	0.37	0.21	0.39	0.27

minerals include tourmaline, zircon, monazite, apatite, opaque oxides, sphene and allanite. Centimetre/decimetre-sized metasedimentary country rock xenoliths are present in the periphery of the pluton. In addition, mafic and hybrid enclaves indicate mingling and mixing processes during granite emplacement.

As shown by Stutz & Thöni (1987) the Nyimaling granitic pluton in the Tso Morari culmination about 5 km southwest of the Indus Yarlung Suture Zone intrudes early Cambrian quartzites and dolomites. Additional samples were collected along the road near Runtse and north of Pang. These include tourmaline–leucogranites and coarse-grained two-mica granites containing pseudomorphs after cordierite.

4. Major, trace element and isotope geochemistry

The Mandi granites are peraluminous (A/CNK = 1.03–1.23) with SiO_2 varying between 66–75% and relatively rich in K_2O, Rb and Th (Table 2). The granite is characterized by chondrite-normalized rare earth element (REE) distributions that are preferentially enriched in light REE (La_N/Lu_N = 14.6–34.6) and show pronounced negative Eu anomalies (Eu/Eu* = 0.19–0.37). REE contents of the granitoids from the outcrop where mingling structures were observed (289–483 ppm) and the non-porphyritic granites (53–79 ppm) are quite distinct and do not correlate with SiO_2, being controlled by minerals such as allanite,

Table 3. Sr isotopic data for late Proterozoic and earIy Palaeozoic granitic rocks, Northwest Himalaya

Sample no.	Locality	Lithology	Rb (ppm)	Sr (ppm)	$^{87}Rb/^{86}Sr$	$^{87}Sr/^{86}Sr \pm 2\sigma$
HF89/90	Mandi	Diorite	38	254	0.43	0.71350 ± 20
HF06/92	Chandra	Bi–Ms granite	327	54	17.70	0.84126 ± 10
HF07/92	Chandra	Bi–Ms granite	303	77	11.54	0.79855 ± 6
HF08/92	Chandra	Bi–Ms granite	361	46	23.10	0.88874 ± 18
HF09/92	Chandra	Bi–Ms granite	301	67	13.22	0.80850 ± 5
HF10/92	Chandra	Leucogranite	413	13	99.80	1.38429 ± 11
HF11/92	Chandra	Leucogranite	473	29	48.10	1.03333 ± 5
HF13/92	Chandra	Bi granite	289	56	15.06	0.82475 ± 6
HF15/92	Chandra	Bi–Ms granite	572	52	32.70	0.93822 ± 8
HF16/92	Chandra	Bi granite	296	85	10.25	0.79088 ± 9
HF17/92	Chandra	Bi–Ms granite	382	68	16.50	0.86964 ± 2
HF18/92	Chandra	Bi granite	251	89	8.24	0.77688 ± 5
HF22/92	Chandra	Bi–Ms granite	339	87	11.40	0.82761 ± 10
HF142/90	Kaplas	Bi–Ms granite	282	91	9.10	0.78841 ± 11
HF143/90	Kaplas	Bi–Ms granite	257	104	7.20	0.76307 ± 12
HF145/90	Kaplas	Bi–Ms granite	277	31	26.79	0.89791 ± 8
PG9180	Kaplas	Bi–Ms granite	261	94	8.06	0.76950 ± 5
PG9136	Kaplas	Bi–Ms granite	364	48	22.37	0.86910 ± 8
PG9137	Kaplas	Bi–Ms granite	366	49	22.13	0.86290 ± 7
HF68/91	Nyimaling	Bi–Ms granite	285	76	11.02	0.79587 ± 12
HF69/91	Nyimaling	Bi–Ms granite	332	43	26.35	0.90362 ± 11
HF70/91	Nyimaling	Bi–Ms–Grt granite	283	65	12.90	0.82162 ± 132
HF01/91	Hanumantibba	Bi granite	181	154	3.41	0.74243 ± 1
WAP28	Chamba	Bi–Ms granite	319	79	11.56	0.80595 ± 80
HF29/92	Kinnaur	Bi–Ms granite	210	85	7.19	0.76443 ± 1
HF30/92	Kinnaur	Bi–Ms granite	204	123	4.84	0.75242 ± 6
HF31/92	Kinnaur	Bi granite	200	115	5.05	0.74759 ± 1
HF32/92	Kinnaur	Leucogranite	265	51	15.10	0.82164 ± 12

Bi = biotite, Ms = muscovite, Grt = garnet.

sphene or apatite. Regression of whole-rock Rb–Sr isotope data (Tables 3, 4) yielded an initial $^{87}Sr/^{86}Sr$ ratio of 0.7112. Initial εNd values range at –9.1 to –10.4 (Table 4).

The Mandi mafic rocks are tholeiitic and olivine-normative, with Mg number between 58 and 77 [Mg no. = $100Mg/(Mg + Fe^{2+})$, setting $Fe^{3+}/Fe^{2+} = 0.15$]. The variations of Cr (248–525 ppm) and Ni (82–198 ppm) relative to MgO suggest fractionation of olivine and pyroxene. All mafic rocks are light REE enriched ($La_N/Lu_N = 2.52–3.94$) with REE contents of 47–102 ppm (Fig. 3a, Table 2). No Eu anomaly was observed. Their mantle-normalized trace element patterns are characterized by large ion lithophile element (LILE) enrichments and by depletions of Ba relative to Rb and Th, and of Nb and Ta relative to La and K (Fig. 3b). The whole rock $\delta^{18}O$ values for the Mandi mafic rocks are 6.4–7.4‰, which is somewhat above the upper mantle values of 5.7 ± 0.5‰ seen in MORB (Kyser, O'Neil & Carmichael, 1982). The initial $^{87}Sr/^{86}Sr$ ratios and εNd values are in the range 0.70354 to 0.70533 and +1.0 to –2.8, respectively (Table 4).

The Kaplas granite samples are predominantly peraluminous (A/CNK = 0.99–1.60) with SiO_2 between 69.5–74.6% (Table 5). CIPW-normative corundum is 0.28–4.48. The chondrite-normalized REE pattern is typical of magmas from a feldspar-bearing but garnet-free crustal source. The $^{87}Sr/^{86}Sr$ initial ratio is 0.7199, based on regression of the whole-rock Rb–Sr data listed in Tables 3 and 4. Only one Kaplas sample was analysed for Sm–Nd isotopes, yielding an initial εNd value of –8.7 (Table 4).

All analysed samples of the Chamba-Kullu-Lahul-Chandra granitic suites (Table 5) are peraluminous (A/CNK = 1.04–1.81) and corundum normative (0.6–6.6%). The chondrite-normalized REE patterns are sloped with LREE enrichment (Ce > 30 times chondritic) and negative Eu anomalies (Eu/Eu* = 0.53–0.77). $^{87}Sr/^{86}Sr$ initial ratios are generally > 0.711 (Tables 3, 4); initial εNd ratios for three samples are –9.3 to –10.1 (Table 4).

The Kinnaur Kailas samples (Table 5) are peraluminous (A/CNK = 1.07–1.46; normative corundum = 1.2–4.9). The chondrite-normalized REE patterns show LREE enrichment ($La_N/Yb_N = 2.0–13.5$) and negative Eu anomalies (Eu/Eu* = 0.3–0.5). Kwatra *et al.* (1999) reported a $^{87}Sr/^{86}Sr$ initial ratio of 0.737 based on five whole rock samples. The Sm–Nd analyses yielded initial εNd values of –7.8 and –13.1 (Tables 1, 4).

The Nyimaling granite samples (Table 5) are highly evolved (71.2–75.8 wt% SiO_2), peraluminous (A/CNK = 1.09–1.27) and corundum normative (1.4–3.5%). The REE show low to moderate fractionation patterns and negative Eu anomalies. According to Stutz & Thöni (1987) the Nyimaling initial $^{87}Sr/^{86}Sr$ ratio is 0.7365. An initial εNd value of –9.3 (Table 4) was determined on a cordierite granite.

Table 4. O, Sr and Nd isotopic data for late Precambrian to early Palaeozoic granitic and mafic rocks and Proterozoic metasediments, Northwest Himalaya

Sample no.	Locality	Lithology	$\delta^{18}O$	Age (Ma)	Rb (ppm)	Sr (ppm)	$^{87}Rb/^{86}Sr$	$^{87}Sr/^{86}Sr \pm 2\sigma$	$^{87}Sr/^{86}Sr(i)$	Sm (ppm)	Nd (ppm)	$^{147}Sm/^{144}Nd$	$^{143}Nd/^{144}Nd \pm 2\sigma$	ε(t) Nd (CHUR)	T(Nd)DM (Ga)
Magmatic rocks															
KAW883	Mandi	Bi–Ms granite	11.6	496	487	14	73.540	1.21300 ± 25	***	3.6	14.5	0.148	0.511949 ± 7	–10.4	2.39
HF67/91	Mandi	Bi–Ms granite	11.2	496	467	21	67.405	1.17580 ± 7	***	3.7	14.9	0.149	0.511954 ± 9	–10.3	2.41
HF63/91	Mandi	Bi granite	9.9	496	257	114	6.560	0.76156 ± 7	0.71519	10.7	53.6	0.121	0.511927 ± 11	–9.1	1.79
HF64/91	Mandi	Granodiorite	9.8	496	315	152	6.075	0.75603 ± 13	0.71309						
HF94/90	Mandi	Qtz diorite	8.5	496	155	196	2.297	0.72480 ± 11	0.70856						
HF66b/91	Mandi	Mafic pillow	7.4	496	76	244	0.907	0.71174 ± 7	0.70533	5.2	21.7	0.145	0.512327 ± 8	–2.8	1.56
HF59/91	Mandi	Mafic pillow	6.5	496	56	249	0.648	0.70812 ± 9	0.70354	4.6	17.4	0.159	0.512569 ± 12	1.0	1.32
HF61/91	Mandi	Mafic pillow	6.4	496	19	275	0.201	0.70547 ± 10	0.70405	2.6	9.9	0.155	0.512531 ± 12	0.6	1.32
HF61/91	Mandi	Plg		496						0.3	1.5	0.109	0.512380 ± 6	0.5	
HF61/91	Mandi	Cpx		496						3.5	9.0	0.233	0.512786 ± 6	0.4	
HF92/90	Mandi	Mafic pillow	6.9	496	76	228	0.961	0.71200 ± 13	0.70521						
HF95/90	Mandi	Mafic pillow	6.8	496	25	270	0.265	0.70750 ± 3	0.70563						
HB06/97	Kinnaur Kailas	Leucogranite		488	413	42	28.969	0.89394 ± 9	***	2.2	7.7	0.1727[a]	0.511891 ± 13	–13.1	3.75**
HB18/97	Kinnaur Kailas	Bi–Ms granite		488	206	106	5.650	0.75703 ± 7	0.71774	8.8	39.6	0.1343[a]	0.512037 ± 3	–7.8	1.87
HF05/92	Chandra	Bi–Ms granite		500*	353	64	16.110	0.82849 ± 7	***	7.1	32.7	0.130	0.511963 ± 6	–8.9	1.90
HF73/91	Nyimaling	Crd granite		460						5.7	25.2	0.136	0.511981 ± 5	–9.3	2.00
HF144/90	Kaplas	Bi–Ms granite		554	356	74	14.000	0.81845 ± 20	0.70828	12.5	75.4	0.099	0.511836 ± 6	–8.7	1.58
WAP25	Hanumantibba	Bi granite		500*	180	114	3.560	0.74740 ± 80	0.72203	4.1	20.3	0.121	0.511920 ± 8	–9.2	1.80
T41	Jaspa	Ms granite		496	484	31	44.553	1.02645 ± 80	0.71157	2.6	9.5	0.166	0.512020 ± 11	–10.1	2.96**
Neoproterozoic metasediments															
WAP2069	NW Tindi	Haimanta Fm.		500*	128	89	4.200	0.76268 ± 10	0.73275	6.4	32.9	0.118	0.511935 ± 2	–8.7	1.72
WAP2070	Miyar valley	Haimanta Fm.		500*	181	154	3.420	0.75009 ± 14	0.72572	7.9	40.9	0.116	0.511676 ± 3	–13.6	2.06
WAP2071	Dhali	Simla Slates		500*	144	64	6.560	0.76399 ± 41	0.71725	6.6	34.5	0.115	0.511850 ± 4	–10.2	1.80
WAP2072	Mashobra	Simla Slates		500*	87	99	2.560	0.74474 ± 14	0.72650	7.7	34.1	0.136	0.511940 ± 4	–9.7	2.06
WAP2073	NE Marwa	Haimanta Fm.		500*	170	197	2.510	0.74165 ± 8	0.72377	8.3	40.0	0.126	0.512058 ± 7	–6.8	1.67
WAP2074	E Udaipur	Haimanta Fm.		500*	91	268	0.980	0.73450 ± 5	0.72752	7.9	38.5	0.125	0.511685 ± 5	–14.0	2.23
WAP2075	Khanderghat	Simla Slates		500*	92	52	5.170	0.77312 ± 8	0.73628	14.9	71.5	0.126	0.511765 ± 10	–12.5	2.13
WAP2076	Naldera	Simla Slates		500*	64	113	1.630	0.72809 ± 9	0.71648	4.9	25.4	0.116	0.511872 ± 6	–9.8	1.78

* Age assumed for calculating initial ratios; *** Rb–Sr system disturbed; Bi = biotite, Cpx = clinopyroxene, Crd = cordierite, Ms = muscovite, Plg = plagioclase, Qtz = quartz; ** See text for explanation of anomalous Nd model ages; [a]Based on Nd and Sm concentrations determined by ICP-MS.

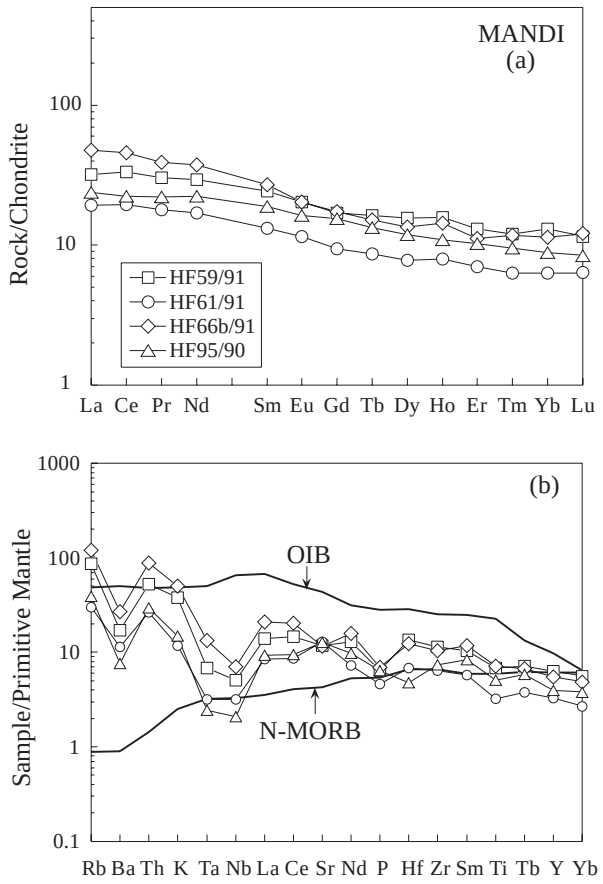

Figure 3. (a) Chondrite-normalized (Boynton, 1984) REE patterns for mafic rocks from Mandi. (b) Primitive mantle normalized trace element variation diagram for mafic rocks from Mandi, Northwest Himalaya. Values for N-MORB, ocean island basalts (OIB) and normalization factors are from Sun & McDonough (1989).

5. *P–T* conditions

Temperature estimates based on zircon solubilities in felsic liquids (Watson & Harrison, 1983) range from 690–817 °C (Mandi granites), 680–750 °C (Kaplas), 670–780 °C (Chamba–Kullu), 743–815 °C (Chandra), 705–802 °C (Nyimaling) and 700–815 °C (Kinnaur Kailas). These temperature estimates are close to conditions required for vapour-absent melting of biotite (e.g. Patiño Douce & Johnston, 1991). The *P–T* conditions recorded by the thermal metamorphism at the base of the Kaplas intrusion are 650–700 °C and 400–500 MPa. Contact metamorphic assemblages containing andalusite also suggest emplacement at pressures ≤ 500 MPa for other plutons. The presence of primary muscovite indicates water-rich melts (e.g. Holtz, 1989).

6. Geochronology

Published Rb–Sr isotope data document wide-spread late Precambrian to early Palaeozoic acid magmatism in the Northwest Himalaya (Table 1). Although the studied granites (Tables 3, 4) plot on a regression line in a $^{87}Rb/^{86}Sr$ vs. $^{87}Sr/^{86}Sr$ diagram indicating an 'age' of 471 ± 21 Ma (Fig. 4a), they do not define an isochron. The scatter in the data may reflect isotopic heterogeneity of source materials, mixing processes, contamination of the magmas during ascent and emplacement, and also open-system behaviour in this overprinted terrain.

In order to better constrain the timing of the felsic magmatism, zircons from the Kaplas intrusion were dated. The U–Pb analysis of six highest-quality, pink magmatic zircon crystals, devoid of any inclusions or visible core features, resulted in a concordia age of 553.2 ± 2.2 Ma (2σ) (Fig. 5; Table 6). This latest Precambrian age is interpreted as dating the magmatic formation of the Kaplas intrusion. In contrast, the two colourless zircons are highly discordant, indicating some major zircon inheritance with $^{207}Pb/^{206}Pb$ minimum ages of *c.* 1100 Ma (Fig. 5; Table 6). In contrast, the Rb–Sr whole rock age of the Kaplas granite is 476 ± 12 Ma, suggesting that Rb–Sr systematics in this complex terrain reveal little more than the presence of late Precambrian/early Palaeozoic event(s). Therefore most Rb–Sr ages listed in Table 1 should be viewed with caution.

In addition, Sm–Nd isotopic data were determined for three gabbro samples from the Mandi mingling complex (Table 4) which exhibits evidence for contemporaneous generation of mafic and granitic magmas. Samples HF59/91 and HF61/91 have similar Sm/Nd ratios and Nd isotope characteristics with slightly negative present-day εNd values (–1.4 to –2.1). For sample HF61/91, the whole rock, plagioclase and clinopyroxene separates have been analysed. If regressed as a separate set, these three data points yield a Sm–Nd age of 496 ± 14 Ma (MSWD = 0.018) and a corresponding initial εNd value of +0.55 (Fig. 4b). The Nd depleted mantle model ages of the Mandi mafic rocks range from 1.3 to 1.6 Ga, the higher age being correlated with a higher Sr initial ratio (Table 4). In contrast, most of the analysed late Precambrian to early Palaeozoic granites are characterized by Nd depleted mantle model ages that range from *c.* 1.6 to 2.4 Ga (Table 4), indicating crustal sources with a minimum mid- to early Proterozoic crustal residence age. Samples HB06/97 (Kinnaur Kailash) and T41 (Jaspa), however, have distinctly older depleted mantle model ages (Table 4). These evolved silicic samples also have relatively low Nd and Sm contents, coupled with relatively high $^{147}Sm/^{144}Nd$ ratios. As suggested previously (e.g. Miller & Mittelfehldt, 1982; Liew & McCulloch, 1985; Hoinkes *et al.* 1997), these isotopic characteristics could indicate fractionation of LREE-rich phases (e.g. monazite) during magma formation in the crust, resulting in anatectic melts with high Sm/Nd ratios and, hence, anomalously high apparent model Nd ages.

Table 5. Major (wt %), trace element and REE (ppm) concentrations of late Proterozoic and early Palaeozoic granitic rocks, Northwest Himalaya

Sample no.	WAP25	HF98/90	HF143/90	HF144/90	HF73/91	HF05/92	HB06/97	HB18/97	HB25/97	HB26/97
Location	H. Tibba	Baragran	Kaplas	Kaplas	Nyimaling	Chandra	Kinnaur K	Kinnaur K	Kinnaur K	Kinnaur K
SiO_2	68.01	73.7	69.83	70.95	72.40	71.83	71.65	69.73	69.27	74.92
TiO2	0.39	0.17	0.50	0.45	0.45	0.35	0.11	0.65	0.58	0.13
Al_2O_3	14.68	13.50	13.86	14.58	13.39	13.92	15.55	13.89	13.89	13.92
Fe_2O_3	3.55	1.88	3.71	3.14	2.87	2.93	0.81	4.46	4.13	0.88
MnO	0.06	0.06	0.04	0.03	0.07	0.06	0.05	0.06	0.08	0.09
MgO	1.62	0.52	0.89	0.67	0.85	0.74	0.02	1.14	1.11	0.06
CaO	2.68	1.36	1.91	0.91	1.06	1.23	0.65	2.13	2.02	0.80
Na_2O	2.28	2.82	3.58	2.10	2.92	2.74	3.63	2.42	2.72	3.04
K_2O	4.54	4.39	4.28	5.10	4.61	4.54	4.98	4.06	4.44	4.85
P_2O_5	0.10	0.09	0.17	0.18	0.16	0.23	0.34	0.19	0.14	0.07
LOI	0.81	0.43	0.45	0.93	1.18	0.64	1.43	0.79	0.75	0.65
Total	98.72	98.92	99.22	99.04	99.96	99.21	99.22	99.52	99.13	99.41
F	883	636	1152	1620	n.d.	n.d.	490	530	400	200
Be	3.6	6.6	3.4	3.5	n.d.	1.4	<20	<20	<20	<20
Sc	9	6	9	6	n.d.	7	3	9	10	5
V	63	23	56	43	31	51	3	61	40	50
Cr	73	57	105	75	49	40	6	30	24	14
Co	12	3	9	7	2	2	1	8	8	1.7
Ni	30	7	5	3	11	13	0.3	10	10	5
Cu	12	0	0	14	10	40	1	12	5	2
Zn	42	26	62	76	50	91	64	67	50	62
Ga	16	17	n.d.	n.d.	n.d.	n.d.	23	20	19	16
Rb	180	260	257	356	359	353	413	206	260	300
Sr	114	70	104	74	46	64	42	106	94	35
Y	17	27	34	10	20	27	12	31	40	50
Zr	116	70	191	225	135	150	46	250	205	78
Nb	3	10	16	9	11	17	17	15	13	8
Ba	986	309	514	469	420	359	128	611	518	138
Hf	0.4	0.3	0.22	n.d.	5	n.d.	1.5	6.9	6.3	3.4
Ta	5.6	1.9	9.6	n.d.	1.8	n.d.	4.9	2.3	1.6	2.4
Pb	24	26	16	17	28	n.d.	33	26	29	34
Th	13	12	34	n.d.	16	n.d.	5.5	27.3	25.7	16.7
U	3.6	4.7	4.5	n.d.	2.2	n.d.	13	3	4	12
La	20	14	53	87	28	34	9	45	39	17
Ce	41	30	106	132	59	73	18	89	80	37
Pr	5.0	3.5	13	18	7	8.8	2	11	10	5
Nd	19	13	56	75	25	32	8	40	37	17
Sm	4.4	3.2	10	12	6	7.3	2	9	7	5
Eu	1.2	0.6	1.3	1.5	0.7	0.8	0.6	1.3	1.1	0.4
Gd	5.1	3.9	10	13	5	5.3	2	7	7	5
Tb	0.46	0.58	1.1	1.5	0.87	0.82	0.4	1.1	1.0	1.0
Dy	2.9	3.6	6.2	8.7	5.3	4.8	2.1	5.8	6.3	7.1
Ho	0.6	0.72	1.1	1.7	1.1	0.88	0.30	1.00	1.23	1.55
Er	1.5	2.1	2.9	3.7	2.4	2.4	0.6	2.7	3.5	4.6
Tm	0.23	0.32	0.37	0.50	0.37	0.35	0.10	0.40	0.55	0.90
Yb	1.27	2.1	2.1	3.1	2.5	2.4	0.5	2.3	3.5	5.7
Lu	0.21	0.28	0.28	0.40	0.32	0.36	0.07	0.40	0.52	0.92

Kinnaur K = Kinnaur Kailash.

7. Discussion

7.a. Source characteristics of silicic igneous rocks

Granitoid rocks can be classified into S-, I-, M- and A-types (e.g. Eby, 1990). The analysed granitoids are peraluminous and corundum normative. These compositional features, Rb/Ba ratios > 0.25, high initial $^{87}Sr/^{86}Sr$ (> 0.7134), high oxygen isotope ratios ($\delta^{18}O$ = 9.6–11.8 ‰) and low initial εNd values (–8.7 to –13.1) point to a major role of recycled continental crust in their source. The peraluminous Nyimaling granites which contain cordierite-pseudomorphs even fit the criteria for S-type granite. The crystallization of magmatic tourmaline is also consistent with a metasedimentary source (Benard, Moutou & Pichavant, 1985).

It has been suggested (Parrish & Hodges, 1996; Whittington *et al.* 1999; Ahmad *et al.* 2000) that the lithological sequences of the High Himalayan Crystalline Series and the Lesser Himalayan Series can be identified along strike of the Himalayan orogen on the basis of their distinct Nd model ages. According to Whittington *et al.* (1999), the High Himalayan Crystalline Series is characterized by depleted mantle model ages in the range of 1.2–2.0 Ga and is distinct from the Lesser Himalayan Series where Nd model

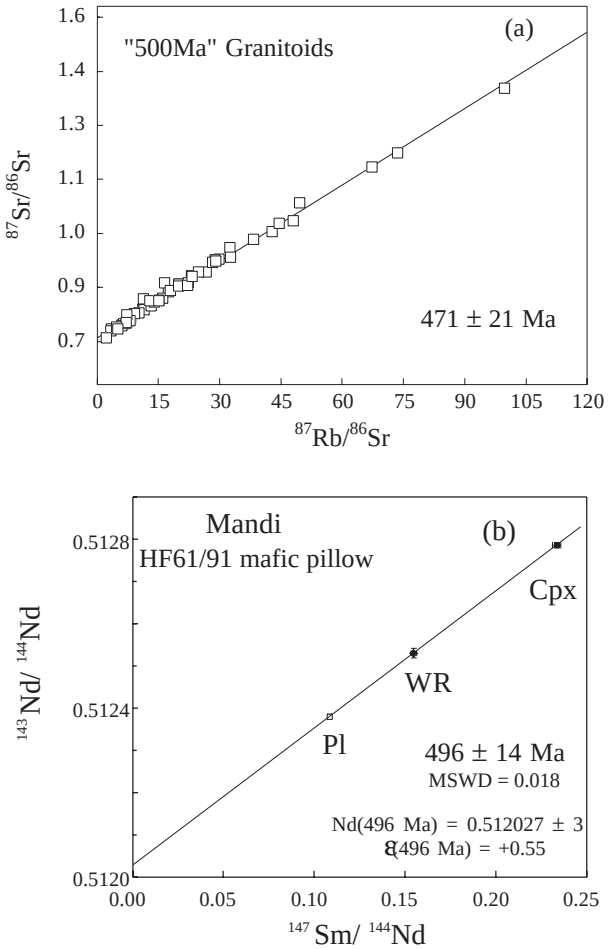

Figure 4. (a) Rb–Sr isochron diagram for 51 early Palaeozoic granitic rocks from the High Himalayan Crystalline Series, Northwest Himalaya, (b) Sm–Nd isochron diagram for plagioclase, clinopyroxene and whole rock of olivine–tholeiite HF61/91 from Mandi mingling complex.

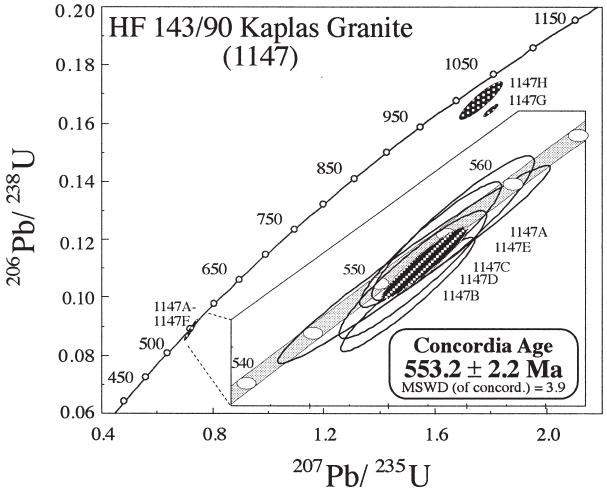

Figure 5. Concordia diagram showing zircon data for Kaplas granite HF143/90. Data-point error ellipses are 2 sigma (*c.* 95% confidence limit). The reported concordia age is calculated using Isoplot/Ex (Ludwig, 1999).

ages range from 2.3–3.4 Ga. Our Sm–Nd data from the Northwest Himalaya (Table 4), however, show that Palaeozoic granites with anomalously old Nd model ages are present within the High Himalayan Crystalline Series and overlap data reported for the Lesser Himalayan Series and the Main Central Thrust Zone. In addition, model ages obtained on flysch-type Neoproterozoic metasediments (Table 4) from the Simla-Blaini-Krol sequence in the Lesser Himalayan Series (1.8–2.1 Ga) and from the Haimanta Group in the High Himalayan Crystalline Series (1.7–2.2 Ga) show considerable overlap, suggesting a similar provenance for these metaclastics in the footwall and hanging wall of the Main Central Thrust.

7.b. Source characteristics of mafic igneous rocks

The Mandi mafic rocks are tholeiitic. Melting experiments (Jaques & Green, 1980) have shown that tholeiitic basalt magmas can be produced from a dry lherzolitic mantle by relatively high degrees (20–30%) of partial melting. Ce/Yb values of 10–12 suggest a garnet-free source. In spite of being relatively magnesian and rich in Cr, they are too poor in Ni to be considered primary magmas. The variations in Cr and Ni with MgO (not shown) suggest fractionation of olivine and clinopyroxene during their evolution. The $^{87}Sr/^{86}Sr$ and $^{143}Nd/^{144}Nd$ ratios of the Mandi mafic rocks plot on the mantle array (Fig. 6), close to Bulk Earth values and within the field of certain oceanic island basalts (OIB). Their trace element signature, however, is clearly different from that of oceanic basalts, showing enrichment in LILE and LREE, and depletion in high field strength elements (Fig. 3b). Negative Nb, Ta and Ti anomalies are not observed in basalts from normal ocean basins (MORB and OIB). They are, however, characteristic features of subduction-related magmas or of continental tholeiites, including flood basalts. The absence of distinctive spikes at Sr and Ba and Ba/La ratios <15 argue against an origin of the Mandi mafic melts at a convergent plate boundary. Sr correlates negatively with K, Rb and Ba, suggesting high-level crustal contamination by low-Sr material such as granitic partial melts. In addition, a continental crustal signature is indicated by geochemical parameters such as Ce/Pb (3.0–4.1) and Nb/U (2.5–7.1) ratios which are distinctly lower than those of oceanic basalts. Crustal contamination of mantle-derived melts is also indicated by weak positive correlations of the initial $^{87}Sr/^{86}Sr$ compositions with Rb/Zr and Rb/Sr ratios, and with $\delta^{18}O$ values (Table 4). These data and Figure 6 show that high-level crustal assimilation probably was an important process during the genesis of some of the Mandi mafic rocks.

Table 6. Single zircon U–Pb data of sample HF143/90 (1147), Kaplas granite, Northwest Himalaya

Sample fraction	Crystal type (a)	Atomic ratios					Apparent ages (Ma)		
		$^{206}Pb/^{204}Pb$ (b)	$^{205}Pb/^{238}U$ ± 2 SD (c)	$^{207}Pb/^{235}U$ ± 2 SD (c)	$^{207}Pb/^{206}Pb$ ± 2 SD (c)	$^{208}Pb/^{206}Pb$ ± 2 SD (c)	$^{206}Pb/^{238}U$ ± 2 SD	$^{207}Pb/^{235}U$ ± 2 SD	$^{207}Pb/^{205}Pb$ ± 2 SD
1147A	Pink, 120 µm, 1:4	18101	0.09001 ± 0.00100	0.72226 ± 0.00843	0.05867 ± 0.00067	0.0660 ± 0.0008	556 ± 6	552 ± 5	555 ± 25
1147B	Pink, 100 µm, 1:4	684	0.08890 ± 0.00079	0.73226 ± 0.00693	0.05894 ± 0.00055	0.0326 ± 0.0003	549 ± 5	558 ± 4	565 ± 20
1147C	Pink, 90 µm, 1:5	35112	0.08940 ± 0.00137	0.72226 ± 0.01410	0.05867 ± 0.00100	0.1213 ± 0.0023	552 ± 8	552 ± 8	555 ± 37
1147D	Pink, 100 µm, 1:4	13924	0.08923 ± 0.00089	0.73247 ± 0.00769	0.05877 ± 0.00061	0.1016 ± 0.0001	551 ± 5	558 ± 5	559 ± 23
1147E	Pink, 100 µm, 1:3	770	0.08974 ± 0.00087	0.72057 ± 0.00730	0.05862 ± 0.00059	0.1612 ± 0.0017	554 ± 5	551 ± 4	553 ± 22
1147F	Pink, 100 µm, 1:3	3275	0.08788 ± 0.00168	0.71887 ± 0.01390	0.05878 ± 0.00113	0.1523 ± 0.0030	543 ± 10	550 ± 8	559 ± 42
1147G	Colourl., 90 µm, 1:2	230	0.16455 ± 0.00157	1.83480 ± 0.01847	0.07944 ± 0.00076	0.1875 ± 0.0002	982 ± 9	1058 ± 7	1183 ± 19
1147H	Colourl., 80 µm, 1:2	501	0.16780 ± 0.00511	1.91406 ± 0.06135	0.07626 ± 0.00208	0.0492 ± 0.0014	1000 ± 28	1086 ± 23	1102 ± 54

(a) Colour, size along c-axes, elongation; (b) corrected for blank-Pb contributions; (c) corrected for blank and common-Pb contributions. All errors are 2 standard deviations.

7.c. Tectonic controls on magma genesis

In the High Himalayan Crystalline Series, the considerable extent of pre-Himalayan large-volume peraluminous silicic magmatism suggests processes of large-scale reworking of continental crust in the Indian part of Gondwana (Table 1). Our age data have a considerable age range, which could be explained by either two granite-producing events, in late Precambrian and in early Ordovician time, or, alternatively, a longer lasting magmatic event covering a time span of more than 50 Ma. Although U–Pb zircon data (Schärer, Xu & Allègre, 1986) and Rb–Sr systematics (e.g. Debon *et al.* 1981) also document melt formation by anatexis of the continental crust in the North Himalaya in the late Precambrian period (Table 1), data are still too few to decide between these possibilities.

Since 'granitic intrusions and transgressive Ordovician sedimentary successions characterize a large area of the Indian part of the Gondwana supercontinent' (Le Fort, Tongiorgi & Gaetani, 1994), a genetic relationship of both processes seems likely. The unconformity below the early Ordovician transgressive event is an important feature in the stratigraphy of the Northwest Himalaya, terminating the Proterozoic–Cambrian Haimanta sedimentary megacycle that comprises more than 5000 m of mainly siliciclastic sediments (Hayden, 1904; Brookfield, 1993). Lithofacies and the Cambrian trilobite fauna suggest an open marine environment on a broad shelf, at least for the uppermost part of the group (Brookfield, 1993; Hughes & Jell, 1999). The cause for the depositional break is not yet known. Above the unconformity, transgression-related conglomerates indicate a fluvial to fluvial-marine environment and have been recorded from the Peshawar basin (Pogue *et al.* 1992), the Karakoram (Le Fort, Tongiorgi & Gaetani, 1994), Spiti (Hayden, 1904) and Kumaun (Heim & Gansser, 1939). Subsequently, thin shelf sediments have been deposited up to the Permian (Bagati, 1991). In spite of some variations in different sections, the depositional gap below the transgression, caused by surface uplift and erosion, lasted from about early late Cambrian to early Ordovician (15–20 Ma) (Le Fort, Tongiorgi & Gaetani, 1994; Bowring & Erwin, 1998; Hughes & Jell, 1999) and coincides with the end of the period of magmatic activity (470–485 Ma; Table 1).

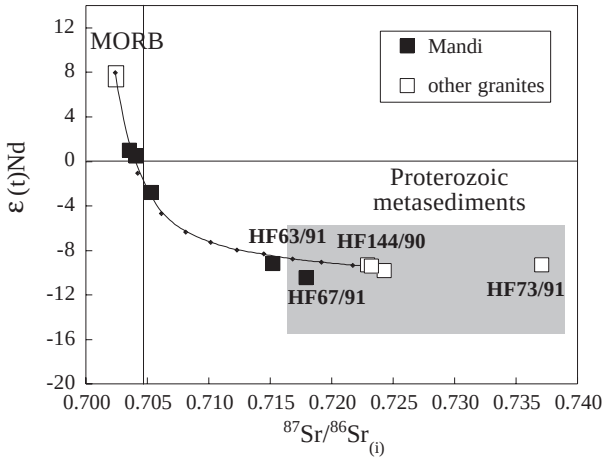

Figure 6. Initial εNd values and $^{87}Sr/^{86}Sr$ ratios for mafic and silicic rocks from Mandi, other late Proterozoic to early Palaeozoic granites and Proterozoic metasediments from the High Himalayan Crystalline Series, Northwest Himalaya. Note that Mandi mafic rocks plot on the mantle array of oceanic basalts. Mixing calculations illustrate the possible effects of bulk assimilation of continental crust. The uncontaminated basalt composition used in modelling has $^{87}Sr/^{86}Sr = 0.70274$, $^{143}Nd/^{144}Nd = 0.513114$, Sr = 90 ppm, Nd = 7.3 ppm. The crustal component is Kaplas granite HF144/90 (Table 4). Points on mixing curve are at 10% intervals.

Considering the fact that the periods of magmatism, surface uplift and erosion are very short compared with the long-lasting slow subsidence of a passive continental margin, and in the absence of any clear evidence for major metamorphism and deformation associated with this Cambro-Ordovician event, a collision-type orogeny seems unrealistic. In addition, the Ordovician conglomerates are mainly composed of detrital components derived from the underlying Haimanta Group. South of Muth (Pin valley, Spiti),

the Ordovician unconformity cuts upright, open mesoscopic folds within the Haimanta Group, constrained also on an even larger scale by balanced cross-section techniques (Wiesmayr *et al.* 1998). Despite these indications of crustal deformation, the transgression of the Ordovician basal conglomerates on a north-west-dipping normal fault within the Haimanta Group (7 km SSE of Muth) indicates a pre-Ordovician age of extensional faulting (Wiesmayr *et al.* 1998). Therefore, lithospheric extension could be a cause for crustal melting as proposed by Le Fort *et al*. (1986). Two processes which result in granitic magma generation should be considered.

(1) It is widely believed that hot mantle-derived melts induce melting of the continental crust (e.g. Hildreth, 1981; Huppert & Sparks, 1988). This mechanism is consistent with an extensional regime; its application requires evidence for commingling of magmas. Although Palaeozoic metagabbros (Pognante *et al.* 1990; Wyss, Hermann & Steck, 1999) are rare in the High Himalayan Crystalline Series, mafic enclaves in many of the Palaeozoic granitic plutons and especially the Mandi mingling complex clearly document that mafic magmas did intrude silicic magma reservoirs within the crust. Chemical and isotopic data suggest that the magmas have different sources: the mafic liquids have been generated in the mantle and the granitic magmas from the continental crust. This thermal episode could indicate asthenospheric upwelling and passive crustal extension, possibly even a rift event that separated the proto-Indian margin and cratonic fragments in Asia such as the South China block (e.g. figs 2, 3 in Dalziel, Dalla Salda & Gahagan, 1994).

It is also tempting to correlate the early Palaeozoic magmatic activities in the Northwest Himalaya with a late extensional stage of the long-lasting Pan-African orogenic events which ended with the formation of the Gondwana supercontinent (Girard & Bussy, 1999, and references cited therein). Although the early Palaeozoic granites in the Northwest Himalaya clearly post-date collision and major thermal events in the Pan-African orogen, and palaeogeographic reconstructions suggest that only the southern parts of the Indian plate were affected by the main Pan-African event (e.g. Stern, 1994), the faults bounding the vast infra-Cambrian to mid-Cambrian evaporite basins of central Iran could have been related to a late Pan-African Basin-and-Range type rift cluster that may have affected much of the Gondwana margin between Arabia and northern India (e.g. Şengör & Natal'in, 1996; Şengör, pers. comm.).

(2) An alternative mechanism has recently been proposed by Sandiford, Hand & McLaren (1998) for the Mount Painter province in Australia. There, the Neoproterozoic sediments of the Adelaide geosyncline have been deposited over several hundred million years during extension-related thermal subsidence. This was terminated during a regional basin inversion event at *c.* 500 Ma, associated with a high geothermal gradient metamorphism (Jenkins, 1991). Burial of sequences enriched in heat-producing elements during thermal subsidence produces high geothermal gradients in the overlying sedimentary successions. This process also increases the depth extent of the high geothermal gradients in the mid-upper crust, potentially promoting conditions for crustal melting. However, the presence of tholeiitic mafic rocks argues against this scenario without input of mantle material.

8. Conclusions

In the High Himalayan Crystalline Series, latest Proterozoic and Ordovician peraluminous granitic intrusions record pre-Himalayan anatectic events in the continental crust. For the early Ordovician Mandi granite, our work documents the involvement of tholeiitic mafic melts and, hence, an important process of mantle-derived heat and mass transfer, possibly resulting in crustal melting and the generation of granitic magmas. Sm–Nd systematics of the syn-plutonic mafic rocks in the Mandi granite date this event at 496 ± 14 Ma. For the Kaplas granite, zircon U–Pb dating yielded a concordia age of 553 ± 2 Ma, which we interpret as the age of magmatism, and which is considerably older than the age indicated by the internal Rb–Sr isochron (472 Ma). A similar age discrepancy is seen in the data published for the Kangmar dome orthogneiss, where the U–Pb age indicates 562 ± 4 Ma for the protolith (Schärer, Xu & Allègre, 1986) in contrast to 483 ± 7 Ma based on Rb–Sr systematics (e.g. Debon *et al.* 1981). This clearly shows that additional high-precision age data are needed in order to improve the resolution of the timing and duration of the pre-Himalayan igneous activities and insight into processes responsible for large-scale crustal anatexis and granite intrusions that seem to have stabilized the northern part of the former passive margin of India.

Acknowledgements. Field studies were financed by the Fonds zur Förderung der wissenschaftlichen Forschung (FWF), projects P7499-GEO and P11765-GEO. We thank S. Hoernes (Bonn) for providing the oxygen isotope analyses and M. Jelenc (Vienna) for her help with Sr isotope analyses. We gratefully acknowledge the critical comments by R. Parrish and M. Sandiford which improved the original draft.

References

Ahmad, T., Harris, N., Bickle, M., Chapman, H., Bunbury, J. & Prince, C. 2000. Isotopic constraints on the structural relationships between the Lesser Himalayan Series and the High Himalayan Crystalline Series, Garhwal Himalaya. *Geological Society of America Bulletin* **112**, 467–77.

Bagati, T. N. 1991. Evolution of the Tethyan sedimentary basin in the western Himalaya. In *Sedimentary Basins of India, Tectonic Context* (eds S. K. Tandon, C. C. Pant

and S. M. Casshyap), pp. 218–35. Gyanodaya Prakashan: Nainital.

Benard, F., Moutou, P. & Pichavant, M. 1985. Phase relations of tourmaline leucogranites and the significance of tourmaline in silicic magmas. *Journal of Geology* **93**, 271–91.

Bhanot, V. B., Bhandari, A. K., Singh, V. P. & Kansal, A. K. 1979. Geochronological and geological studies on a granite of Higher Himalaya, northeast of Manikaran, Himachal Pradesh. *Journal of the Geological Society of India* **20**, 90–4.

Blake, D. H., Elwell, R. W. D., Gibson, I. L., Skelhorn, R. R. & Walker, G. P. L. 1965. Some relationships resulting from the intimate association of acid and basic magmas. *Journal of the Geological Society, London* **121**, 31–50.

Bowring, S. A. & Erwin, D. H. 1998. A new look at evolutionary rates in deep time: uniting paleontology and high-precision geochronology. *GSA Today* **8/9**, 2–8.

Boynton, W. V. 1984. Cosmochemistry of the rare earth elements: meteorite studies. In *Rare Earth Element Geochemistry* (ed. P. Henderson), pp. 63–114. Amsterdam: Elsevier.

Brookfield, M. E. 1993. The Himalayan passive margin from Precambrian to Cretaceous times. *Sedimentary Geology* **84**, 1–35.

Burg, J. P. & Chen, G. M. 1984. Tectonics and structural formation of southern Tibet. *Nature* **311**, 219–23.

Dalziel, I. W. D., Dalla Salda, L. H. & Gahagan, L. M. 1994. Paleozoic Laurentia–Gondwana interaction and the origin of the Appalachian–Andean mountain system. *Geological Society of America Bulletin* **106**, 243–52.

Debon, F., Le Fort, P., Sonet, J., Liu, G., Jin, C. & Xu, R. 1981. About the lower Paleozoic age of the Kangmar granite (Lhagoi Kangri plutonic belt, South Tibet, China). *Terra Cognita Special Issue* **14**, 67–8.

Eby, G. N. 1990. The A-type granitoids: a review of their occurrences and chemical characteristics and speculations on their petrogenesis. *Lithos* **26**, 115–34.

Einfalt, H. C., Hoehndorf, A. & Kaphle, K. P. 1993. Radiometric age determination of the Dadeldhura granite, Lesser Himalaya, Far Western Nepal. *Schweizerische Mineralogische und Petrographische Mitteilungen* **73**, 97–106.

Frank, W., Thöni, M. & Purtscheller, F. 1977. Geology and petrography of Kullu–south Lahul area. *Science de la Terre* **268**, 147–72.

Frank, W., Grasemann, B., Guntli, P. & Miller, C. 1995. Geological map of the Kishtwar, Chamba and Kulu region, NW Himalaya, India. *Jahrbuch der Geologischen Bundesanstalt* **138**, 299–308.

Gaetani, M. & Garzanti, E. 1991. Multicycle history of the northern India continental margin (northwestern Himalaya). *American Association of Petroleum Geologists Bulletin* **75**, 1427–46.

Gansser, A. 1964. *Geology of the Himalayas*. London: Interscience Publishers, 289 pp.

Girard, M. & Bussy, F. 1999. Late Pan-African magmatism in the Himalaya: new geochronological and geochemical data from the Ordovician Tso Morari metagranites (Ladakh, NW India). *Schweizerische Mineralogische und Petrographische Mitteilungen* **79**, 399–418.

Hayden, H. H. 1904. The geology of Spiti, with part of Bashar and Rupshu. *Memoirs of the Geological Survey of India* **36**, 1–129.

Heim, A. & Gansser, A. 1939. Central Himalaya – Geological observations of the Swiss expedition 1936. *Memoire Societé Helvetique Science naturelle* **73**, 1–245.

Hildreth, W. 1981. Gradients in silicic magma chambers: Implications for lithospheric magmatism. *Journal of Geophysical Research* **86**, 10153–92.

Hoinkes, G., Thöni, M., Lichem, C., Bernhard, F., Kaindl, R., Schweigl, J., Tropper, P. & Cosca, M. 1997. Metagranitoids and associated metasediments as indicators for the pre-Alpine metamorphic evolution of the western Ötztal Basement (Kaunertal, Tirol). *Schweizerische Mineralogische und Petrographische Mitteilungen* **77**, 299–314.

Holtz, F. 1989. Importance of melt fraction and source rock composition in crustal genesis – the example of two granitic suites of northwestern Portugal. *Lithos* **24**, 21–35.

Hughes, N. C. & Jell, P. A. 1999. Biostratigraphy and biogeography of Himalayan Cambrian trilobites. In *Himalaya and Tibet – Mountain Roots to Mountain Tops* (eds A. Macfarlane, R. B. Sorkhabi and J. Quade), pp. 109–16. Geological Society of America, Special Paper no. 328.

Huppert, H. E. & Sparks, R. J. 1988. The generation of granitic magmas by intrusion of basalt into continental crust. *Journal of Petrology* **29**, 599–624.

Jäger, E., Bhandari, A. K. & Bhanot, V. B. 1971. Rb–Sr age determinations on biotites and whole rock samples from the Mandi and Chor granites, Himachal Pradesh, India. *Eclogae Geologicae Helvetiae* **64**, 521–7.

Jaques, A. L. & Green, D. H. 1980. Anhydrous melting of peridotite at 0–15 Kb pressure and the genesis of tholeiitic basalts. *Contributions to Mineralogy and Petrology* **73**, 287–310.

Jenkins, R. F. J. 1991. The Adelaide foldbelt. A tectonic reappraisal. *Geological Society of Australia Special Publication* **16**, 296–420.

Krogh, T. E. 1982. Improved accuracy of U–Pb ages by the creation of more concordant systems using an air abrasion technique. *Geochimica et Cosmochimica Acta* **46**, 637–49.

Kwatra, S. K., Singh, S., Singh, V. P., Sharma, R. K., Rai, B. & Kishor, N. 1999. Geochemical and geochronological characteristics of the Early Palaeozic granitoids from Sutlej-Baspa Valleys, Himachal Himalaya. *Gondwana Research Group Memoirs* **6**, 145–58.

Kyser, T. K., O'Neil, J. R. & Carmichael, S. E. 1982. Genetic relations among basic lavas and ultramafic nodules: evidence from oxygen isotope compositions. *Contributions to Mineralogy and Petrology* **81**, 88–102.

Le Fort, P., Debon, F. & Sonet, J. 1980. The "Lesser Himalayan" cordierite belt: typology and age of the pluton of Mansehra (Pakistan). *Geological Bulletin of the University of Peshawar Special Issue* **13**, 51–61.

Le Fort, P., Debon, F. & Sonet, J. 1983. The Lower Paleozoic "Lesser Himalayan" granitic belt: emphasis on the Simchar pluton of Central Nepal. In *Granites of Himalayas, Karakorum and Hindu Kush* (ed. F. A. Shams), pp. 235–55. Lahore, Pakistan: Punjab University.

Le Fort, P., Debon, F., Pêcher, A., Sonet, J. & Vidal, P. 1986. The 500 Ma magmatic event in Alpine southern Asia, a thermal episode at Gondwana scale. *Sciences de la Terre, Mémoire* **47**, 191–209.

Le Fort, P., Tongiorgi, M. & Gaetani, M. 1994. Discovery of a crystalline basement and Early

Ordovician marine transgression in the Karakorum mountain range, Pakistan. *Geology* **22**, 941–4.

Liew, T. C. & McCulloch, M. T. 1985. Genesis of granitoid batholiths of Peninsular Malaysia and implications for models of crustal evolution: evidence from a Nd–Sr isotopic and U–Pb zircon study. *Geochimica et Cosmochimica Acta* **49**, 587–600.

Ludwig, K. R. 1999. Isoplot/Ex, a geochronological toolkit for Microsoft Excel. *Berkeley Geochronology Center, Special Publication* **1a**, 49 pp.

Marquer, D., Chawla, H. S. & Challandes, N. 2000. Pre-Alpine high-grade metamorphism in High-Himalaya crystalline sequences: evidence from Lower Palaeozoic Kinnaur Kailash granite and surrounding rocks in the Sutlej Valley (Himachal Pradesh, India). *Eclogae Geologicae Helvetiae* **93**, 207–20.

Michard, A., Gurriet, P., Soudant, M. & Albarede, F. 1985. Nd isotopes in French Phanerozoic shales: external vs. internal aspects of crustal evolution. *Geochimica et Cosmochimica Acta* **49**, 601–10.

Miller, C., Klötzli, U., Frank, W., Thöni, M. & Grasemann, B. 2000. Proterozoic crustal evolution in the NW Himalaya (India) as recorded by circa 1.80 Ga mafic and 1.84 Ga granitic magmatism. *Precambrian Research* **103**, 191–206.

Miller, C., Schuster, R., Klötzli, U., Frank, W. & Purtscheller, F. 1999. Post-collisional potassic and ultrapotassic magmatism in SW Tibet: geochemical and Sr–Nd–Pb–O isotopic constraints for mantle source characteristics and magma genesis. *Journal of Petrology* **40**, 1399–1424.

Miller, C. F. & Mittelfehldt, D. W. 1982. Depletion of light rare-earth elements in felsic magmas. *Geology* **10**, 129–33.

Murphy, J. B. & Nance, R. D. 1991. Supercontinent model for the contrasting character of Late Proterozoic orogenic belts. *Geology* **19**, 469–72.

Parrish, R. R. & Hodges, K. V. 1996. Isotopic constraints on the age and provenance of the Lesser and Greater Himalayan sequences, Nepalese Himalaya. *Geological Society of America Bulletin* **108**, 904–11.

Parrish, R. R., Roddick, J. C., Loveridge, W. D. & Sullivan, R. W. 1987. Uranium-lead analytical techniques at the analytical laboratory, Geological Survey of Canada. *Geological Survey of Canada Paper* **87-2**, 3–7.

Patiño Douce, A. E. & Johnston, A. D. 1991. Phase equilibria and melt productivity in the pelitic system: implications for the origin of peraluminous granitoids and aluminous granulites. *Contributions to Mineralogy and Petrology* **107**, 202–18.

Pognante, U., Castelli, D., Benna, P, Genovese, G., Oberli, F., Meier, M. & Tonarini, S. 1990. The crystalline units of the High Himalayas in the Lahul-Zanskar region (northwest India): metamorphic-tectonic history and geochronology of the collided and imbricated Indian plate. *Geological Magazine* **127**, 101–16.

Pogue, K. R., Wardlaw, B. R., Harris, A. G. & Hussain, A. 1992. Paleozoic and Mesozoic stratigraphy of the Peshawar basin, Pakistan: Correlations and implications. *Geological Society of America Bulletin* **104**, 915–27.

Rai, B., Kwatra, S. K., Singh, V. P. & Sharma, N. K. 1993. Whole rock Rb–Sr age for granitic rocks of Khadrala area, district Shimla, Himachal Pradesh, India. *Preprint Volume 6th National Symposium Mass Spectrometry* **8**, 1–4.

Rao, D. R., Sharma, K. K., Sivaraman, T. V., Gopalan, K. & Trivedi, J. R. 1990. Rb/Sr dating and petrochemistry of Hante granite (Baramulla area) Kashmir Himalaya. *Journal of Himalayan Geology* **1**, 57–63.

Sandiford, M., Hand, M. & McLaren, S. 1998. High geothermal gradient during thermal subsidence. *Earth and Planetary Science Letters* **163**, 149–65.

Schärer, U. & Allègre, C. J. 1983. The Palung granite (Himalaya): high resolution U–Pb systematics in zircon and monazite. *Earth and Planetary Science Letters* **63**, 423–32.

Schärer, U., Xu, R.-H. & Allègre, C. J. 1986. U–(Th)–Pb systematics and ages of Himalayan leucogranites. *Earth and Planetary Science Letters* **77**, 35–48.

Şengör, A. M. C. & Natal'in, B. A. 1996. Paleotectonics of Asia: fragments of a synthesis. In *The Tectonic Evolution of Asia* (eds A. Yin and T. M. Harrison), pp. 486–640. Cambridge: Cambridge University Press.

Sharma, K. K. 1983. Granitoid belts of the Himalaya. In *Granites of Himalayas, Karakorum and Hindu Kush* (ed. F. A. Shams), pp. 11–37. Lahore, Pakistan: Punjab University.

Stern, R. J. 1994. Arc assembly and continental collision in the Neoproterozoic East African Orogen: implications for the consolidation of Gondwana. *Annual Review of Earth and Planetary Sciences* **22**, 319–51.

Stutz, E. & Thöni, M. 1987. The lower Paleozoic Nyimaling granite in the Indian Himalaya (Ladakh): new Rb/Sr data versus zircon typology. *Geologische Rundschau* **76**, 307–15.

Sun, S. S. & McDonough, W. F. 1989. Chemical and isotopic systematics of oceanic basalts: implications for mantle composition and processes. In *Magmatism in the Ocean Basins* (eds A. D. Saunders and M. J. Norry), pp. 313–45. Geological Society of London, Special Publication no. 42.

Trivedi, J. R., Gopalan, K. & Valdiya, K. S. 1984. Rb–Sr ages of granitic rocks within the Lesser Himalayan nappes, Kumaun, India. *Journal of the Geological Society of India* **26**, 641–54.

Vannay, J.-C. & Grasemann, B. 1998. Himalayan inverted metamorphism in the High Himalaya of Kinnaur (NW India): petrography versus thermobarometry. *Schweizerische Mineralogische und Petrographische Mitteilungen* **78**, 107–32.

Wang J., Chen, Z., Gui, X., Xu, R. & Zhang, Y. 1981. Rb–Sr isotopic studies on some intermediate-acid plutons in Southern Xizang. *Proceedings of the Symposium on Qinghai-Xizang (Tibet) Plateau*. Vol. 1, pp. 515–20. Beijing: Science Press.

Watson, E. B. & Harrison, T. M. 1983. Zircon saturation revisited: temperature and composition effects in a variety of crustal magma types. *Earth and Planetary Science Letters* **64**, 295–304.

Wendt, J. I. & Todt, W. 1991. A vapour digestion method for dating single zircons by direct measurement of U and Pb without chemical separation. *Terra Abstracts* **3**, 507–8.

Whittington, A., Foster, G., Harris, N., Vance, D. & Ayres, M. 1999. Lithostratigraphic correlations in the western Himalaya – An isotopic approach. *Geology* **27**, 585–8.

Wiedenbeck, M., Allé, P., Corfu, F., Griffin, W. L., Meier, M., Oberli, I., Quadt, A., Roddick, J. C. &

Spiegel, W. 1995. Three natural zircon standards for U–Th–Pb, Lu–Hf, trace element and REE analyses. *Geostandard Newsletters* **19**, 1–23.

Wiesmayr, G., Grasemann, B., Draganits, E., Frank, W., Fritz, H. & Miller, C. 1998. The main pre-Himalayan and Himalayan deformation phases in the Pin valley (Spiti, Tethyan Himalaya, NW India). *13th Himalaya-Karakoram-Tibet Workshop*, *Geological Bulletin of the University of Peshawar Special Issue* **31**, 212–13.

Wyss, M., Hermann, J. & Steck, A. 1999. Evidence for an early tectonometamorphic event in the High Himalaya Crystalline of the northern Himachal Pradesh. 14th Himalaya-Karakoram-Tibet Workshop, Ettal. *Terra Nostra* **2**, 180–2.